INTERNATIONAL JOURNAL OF CLIMATOLOGY
Int. J. Climatol. **33**: 1470–1481 (2013)
Published online 13 June 2012 in Wiley Online Library
(wileyonlinelibrary.com) DOI: 10.1002/joc.3527

RMetS
Royal Meteorological Society

Climatic response to changes in vegetation in the Northwest Hetao Plain as simulated by the WRF model

Entao Yu,[a,b,c]* Huijun Wang,[a,b] Jianqi Sun[a] and Yongqi Gao[a,d]

[a] *Nansen-Zhu International Research Center, Institute of Atmospheric Physics, Chinese Academy of Sciences, Beijing, China*
[b] *Climate Change Research Center, Chinese Academy of Sciences, Beijing, China*
[c] *Graduate School of the Chinese Academy of Sciences, Beijing, China*
[d] *Nansen Environmental and Remote Sensing Center, Bjerknes Centre for Climate Research, Bergen, Norway*

ABSTRACT: Considering the 'Green Great Wall' project and future climate change, the vegetation in the Northwest Hetao Plain (NWHP) of China is expected to undergo considerable changes. In this study, the climatic response to prescribed changes in vegetation is investigated using the Weather Research and Forecasting model. When the vegetation is changed from 'bare or sparsely vegetated' category to 'grassland' in the NWHP, the climate shows both local and remote responses. Locally, the temperature increases in the winter but decreases in the summer. The precipitation level increases substantially in the summer while increases slightly in the winter, which is mainly caused by the increase in the amount of water-vapour and circulation adjustment. Additionally, atmospheric circulation anomalies also lead to remote circulation responses, including a decrease in precipitation over Central North China and an increase in precipitation over Central and South China. The results of this study bring to light the local and remote climatic responses to changes in vegetation in the NWHP using a state-of-the-art regional climate model.

KEY WORDS vegetation change; climate response; Northwest Hetao Plain

Received 24 July 2011; Revised 29 March 2012; Accepted 5 May 2012

1. Introduction

The Northwest Hetao Plain (NWHP) region, which is located in North China, is a transitional climate zone between the humid monsoon region and the inner arid area. The ecosystem in this area is sensitive to natural climate variability and anthropogenic changes, and is important to the regional climate. Observations show that the annual mean precipitation has been increasing from 1961 to 2000 (Li and Shi, 2009); The Fourth Intergovernmental Panel on Climate Change (IPCC) assessment report projected that precipitation will increase by 10–15% by the end of this century (IPCC, 2007). In addition, the Chinese government has been carrying out the world's largest ecological project, building the 'Green Great Wall' in northern China. By 2050, a total of 35.6 million hectares of land over northern China are planned to be afforested, increasing the region's woodland coverage to 15%. All these natural change and human activity imply that a wide range of areas in the NWHP will likely change from arid area to grassland. If realized, a crucial issue is the maintenance of the grassland and the impacts on the local climate.

Land surface processes can strongly affect climate conditions, and the interaction between local vegetation and climate conditions is an important topic in global change research. The distribution of vegetation is determined by local climatic factors, including precipitation, radiation, and temperature. At the same time, by altering the surface albedo, roughness, and Bowen ratio, land surface changes can significantly alter climate conditions, both regionally and globally (Charney, 1975; Nobre *et al*., 1991; Pielke *et al*., 2002, 2007).

The impact of changes in vegetation (including desertification and afforestation) on climate has been widely investigated in the last three decades, especially for the Sahel desertification and Amazonian deforestation. Charney (1975) first investigated the dynamics of desert and drought in Sahel, and emphasized the role of albedo. More studies followed and confirmed this result (Dickinson and Henderson-Sellers, 1988; Sud and Molod, 1988; Xue and Shukla, 1993, 1996). Other studies (Lean and Warrilow, 1989; Shukla *et al*., 1990; Zhang *et al*., 1996a, 1996b; Wang, 1999; Jiang *et al*., 2001, 2003; Bollasina and Nigam, 2011) focused on more influence factors (e.g. albedo, evaporation, soil moisture, etc.), for example, Wang (1999) highlighted the role of vegetation and soil in the model simulation. Recently, more realistic and complicated numerical simulations were conducted over China, in which multiple parameters (e.g. albedo, green fraction, surface roughness, etc.) were changed along with the vegetation change (e.g. Xue, 1996; Bonan, 1997; Fan *et al*., 1998; Fu and Yuan, 2001; Fu, 2003; Gao *et al*., 2003, 2007; Ding *et al*., 2005; Zeng, 2010). These studies

* Correspondence to: E. Yu, Nansen-Zhu International Research Center, Institute of Atmospheric Physics, Chinese Academy of Sciences, Beijing 100029, China. E-mail: yetsyu@mail.iap.ac.cn

indicate that the climate change caused by land-use practices is comparable to other well-known anthropogenic climate forces. Almost all the previous studies used the global climate model, or were commonly short-term run (one year or less) thus may lead to uncertainty of the results.

What is the climatic response to changes in vegetation in the NWHP in a regional climate model for a sufficient long-term time period? To address this issue, we prescribed an ideal scenario and conducted two 10 year simulations using a regional climate model. The NWHP area was changed from 'bare or sparsely vegetated' category to 'grassland,' with the primary goal of investigating the possible local and remote effects and feedback of changes in vegetation on climate. Such vegetation change is based on the following considerations: first, almost all climate models project an increase in precipitation in this region, which may result in improved vegetation conditions under a global warming scenario; and second, the government's plan of planting trees and grass in this region will help to repair vegetation damage.

This article is organized as follows: section 2 describes the regional model, the observational data used for model validation, and the experimental design. The control simulation results for model validation and the local and remote climatic responses to changes in vegetation in the NWHP are analysed in section 3. A summary and conclusions follow in section 4.

2. Model, data, and experiment design

The Weather Research and Forecasting (WRF, specifically the Advanced Research WRF, WRF-ARW, version 3.2.1) model was used for this simulation. This model is developed in a collaborative effort by the National Center for Atmospheric Research (NCAR), the National Centers for Environmental Prediction (NCEP), the Forecast Systems Laboratory, and other university scientists. More details are described in Skamarock *et al*. (2008). The model has been widely used in weather prediction and long-term simulations (Lo *et al*., 2008; Barstad *et al*., 2009; Qian *et al*., 2010).

The simulation domain covers the entire area of China (Figure 1) with 125 grids along the east–west direction and 96 grids along the north–south direction, with the centre at 38°N, 106°E. The model was used at a horizontal resolution of 60 km and 35 sigma levels, with the model top at 50 hPa. The relevant model parameterizations include the following: WRF Single-Moment 6 class microphysics scheme (WSM6, Hong *et al*., 2004; Hong and Lim, 2006); Kain–Fritsch cumulus convective schemes (Kain and Fritsch, 1993; Kain, 2004); NCAR Community Atmosphere Model Version 3 (CAM3, Collins *et al*., 2004) for shortwave and longwave radiation; Noah Land Surface Model (LSM, Chen and Dudhia, 2001) with four layers of soil temperature and moisture, fractional snow cover and frozen soil physics; and the Yonsei University boundary layer scheme

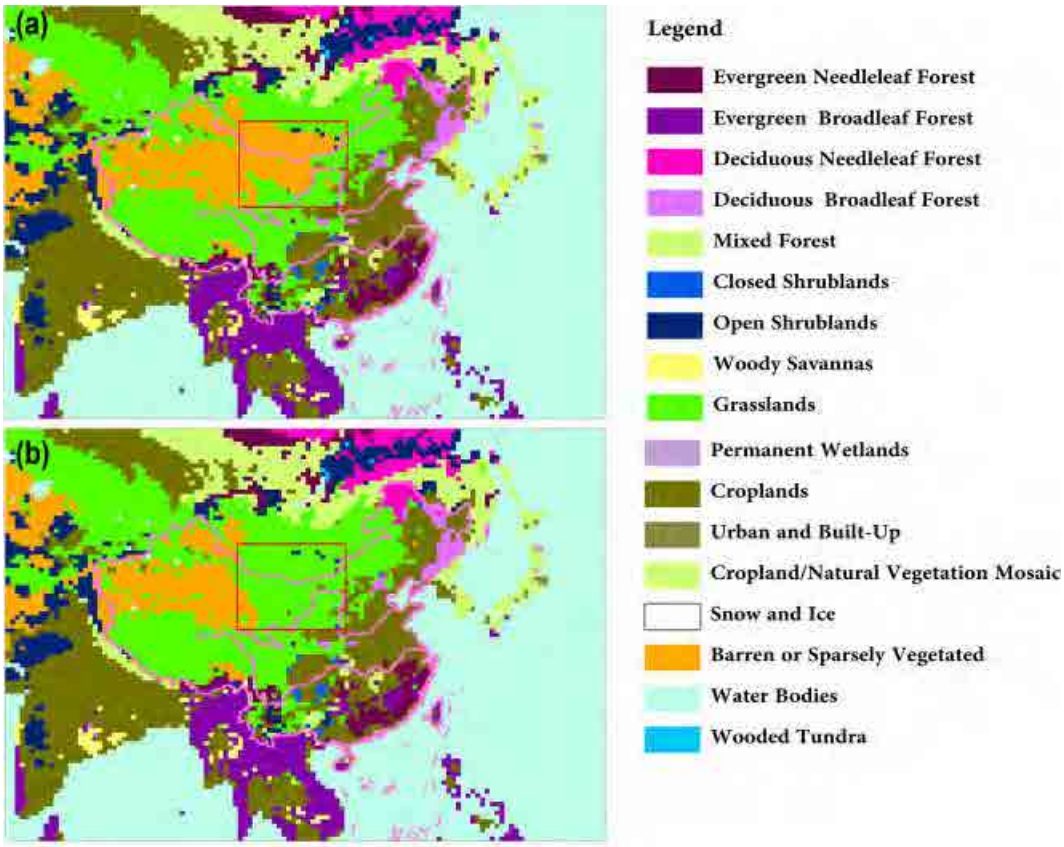

Figure 1. Vegetation distribution of DST and GRS simulations along with the model domain. The red rectangle indicates the NWHP region where the dominant vegetation category changes form 'bare or sparsely vegetated' to 'grassland'.

(Hong *et al.*, 2006). The initial conditions and lateral boundary conditions data were obtained from NCEP Global Final Analysis 6 h data with a horizontal resolution of 1° × 1°. Sea Surface Temperature (SST) data used in this study are from the NCEP real-time global daily SST analysis (RTG_SST, Gemmill *et al.*, 2007) and were linearly interpolated to a 6 h data. Boundary condition, SST and green fraction data were read and updated every 6 h.

The Moderate-resolution Imaging Spectroradiometer 20-category vegetation classification system was used in the Noah LSM. In this study, the dominant vegetation in the NWHP (shown as the red rectangle in Figure 1) was changed from the category 'bare or sparsely vegetated' to the category 'grassland' making the former category cover from 51.04% of the NWHP to 0% and the latter category cover from 43.85 to 94.89%. Along with the change in surface vegetation characteristics, the initial soil moisture, vegetation fraction, and albedo were also modified for consistency. In addition, by changing the vegetation category, many parameters (e.g. root depth, leaf area index, and emissivity) were automatically changed because the Noah LSM assigns the parameter using a lookup table. The simulations of the control run and sensitive runs are referred to as DST (desert) and GRS (grassland), respectively. Table I lists the main changes in the WRF surface parameters, averaged over the NWHP area.

For both DST and GRS, the model was run continuously from 1 December 1999 to 31 December 2009. The result of the first month was considered as the spin-up period and was not analysed (Anthes *et al.*, 1989; Mukhopadhyay *et al.*, 2010). The following 10 year simulation results were used for analysis in this study. The significance of the difference was evaluated by Student's *t*-test.

The surface air temperatures were compared with observational data obtained from the daily gridded temperature data of China Meteorological Administration (cn05) with a horizontal resolution of 0.5° × 0.5°. The cn05 data were constructed based on the interpolation from 751 observation stations in China from 1961 to 2005 (Xu *et al.*, 2009). Observational precipitation data came from the Tropical Rainfall Measuring Mission (TRMM) 3B43 rainfall data set and had a horizontal resolution of 0.25° × 0.25° (Huffman *et al.*, 2001).

Table I. Main changes in parameters averaged over the NWHP for DST and GRS.

Variables (units)		DST	GRS
Vegetation type (%)	Bare or sparsely vegetated	51.04	0
	Grassland	43.85	94.89
Background albedo (–)		0.17	0.14
Green fraction (–)		7.92	24.51
Initial soil moisture (m^3 m^{-3})	0–10 cm	0.19	0.29
	10–40 cm	0.17	0.26
	40–100 cm	0.15	0.19
	100–200 cm	0.16	0.18

3. Results

3.1. Model validation in the region

In this subsection, the simulated surface air temperature and precipitation were compared with observational data to confirm the model's ability to simulate the main climate variables over mainland China. Figure 2 shows the annual mean temperatures from 2000 to 2009 from observations and control runs (DST). The observations (Figure 2(a)) show that except for the Tibetan Plateau, the temperature decreases gradually northward and westward. Higher temperatures occur in southern China, and lower temperatures occur in the Tibetan Plateau and northeastern China. The DST effectively captures the main spatial pattern of the observational annual mean

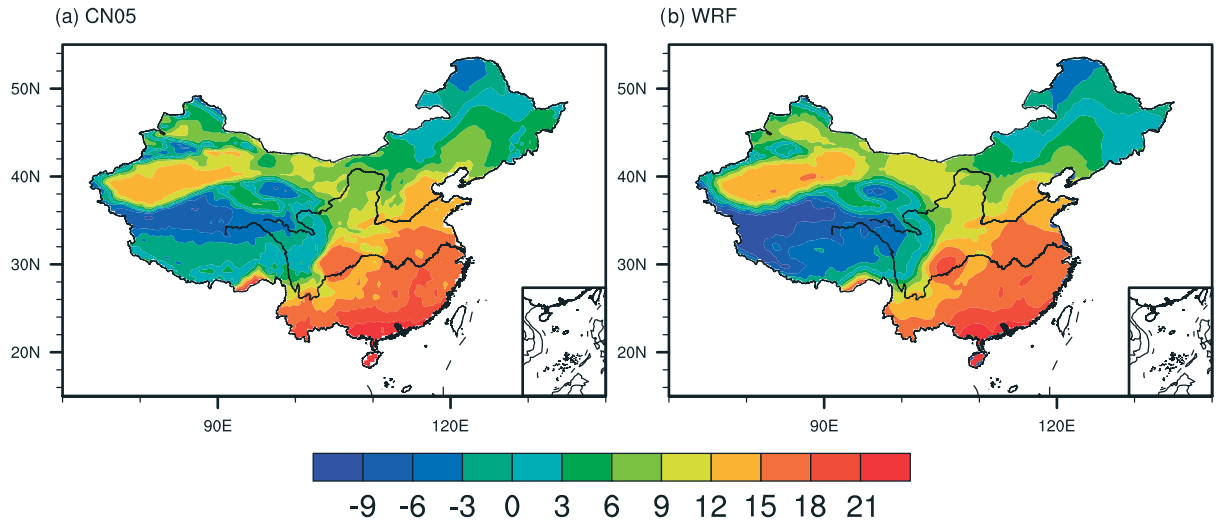

Figure 2. Annual mean temperature derived from the WRF simulation and observations from 2000 to 2009. Unit: °C.

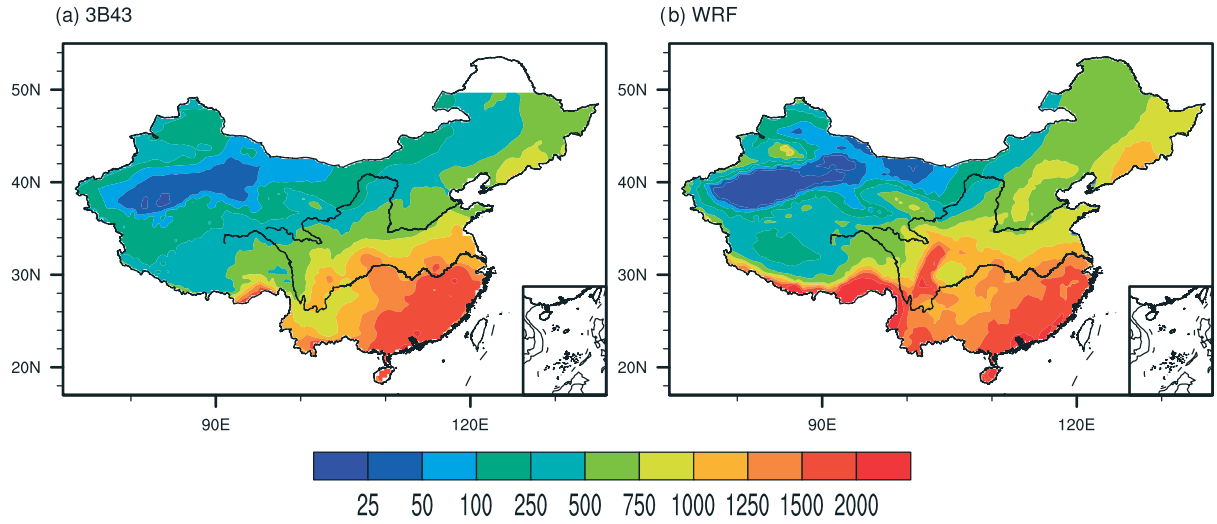

Figure 3. Annual precipitation levels derived from the WRF simulation and observations from 2000 to 2009. Unit: mm a^{-1}.

temperature, and the values over most of mainland China are very close to the observed values. The higher temperatures in southeastern China and over the Tarim Basin and Sichan Basin and the lower temperatures over the Tibetan Plateau and northeastern China are well simulated, except for the cold bias over the Tibetan Plateau which may be related with the complex topography, the spatial correlation coefficient is about 0.96. Thus, the simulation of surface air temperature is in good agreement with observational data.

The DST can also effectively reproduce observational precipitation levels and their spatial distribution (Figure 3). The orographic rain along the southern and southeastern slope of the Himalayas and the shortage of precipitation over the Tarim Basin are effectively reproduced. The simulated boundary of arid and humid areas is in agreement with observational data.

3.2. Climatic response to changes in vegetation over the NWHP

Figure 4 illustrates the annual mean and December–January–February (DJF) and June–July–August (JJA) temperature anomalies (i.e. GRS–DST differences) induced by changes in vegetation. The annual mean air temperature decreased by 0.5 °C in the NWHP, and the JJA temperature change was the main contributor to the annual change over the entire NWHP area. To maintain atmospheric thermal balance, the air temperature around the NWHP area (i.e. areas to the north and south of the NWHP) increased by 0.25 °C. The temperature changes over these areas were relatively unapparent and were caused by temperature increases in both the summer and the winter.

The most conspicuous feature of seasonal temperature change is the local and large-scale responses, especially in JJA, that stretch beyond the NWHP area to almost the entire simulation domain. To analyse the DJF and JJA thermal changes in detail, the anomalies of various components of the surface energy budget are presented in Figure 5. From Figure 4(b), it is clear that the DJF temperature consistently increased by 0.5 °C in the NWHP. Figure 5(e) shows that the DJF upward shortwave radiation flux at the surface decreased substantially in GRS due to the lower albedo (Table I), although the DJF downward shortwave radiation at the surface also decreased (Figure 5(c)) because of the increased cloud fraction (Figure 5(a)), which was induced by the increase in precipitation (Figure 6(b)). The total effect was more solar energy remaining at the surface; as a result, the temperature increased in the winter. Therefore, the temperature change in the winter was physically based, although the magnitude of the change was not highly statistically significant. This simulated change in the DJF temperature would be highly statistically significant if the changes in vegetation were prescribed on a larger spatial scale.

The JJA mean temperature decreased significantly. Figure 4(c) shows that the cooling was centred in the NWHP area. The albedo was also lower, as was true in the winter (i.e. less upward shortwave flux at the surface, Figure 5(d); less downward shortwave radiation, Figure 5(f); and greater cloud fraction, Figure 5(b)). However, we must consider the changes in evapotranspiration, which is another important factor that affects temperature. Vegetation and soil moisture conditions are much more favourable in GRS compared with DST (Table I). The evapotranspiration processes of the vegetation and soil consume large amounts of energy, which is evident from the tremendously increase in surface upward latent heat flux, shown in Figure 5(h). Furthermore, JJA precipitation increased over NWHP (Figure 6(c)), and this favourable condition formed a positive feedback chain between evapotranspiration and precipitation. Consequently, much more energy was consumed, resulting in a decrease in temperature (Figure 4(c)).

The changes in annual, DJF and JJA mean precipitation levels are shown in Figure 6. The remarkable features of local and remote significant responses to changes

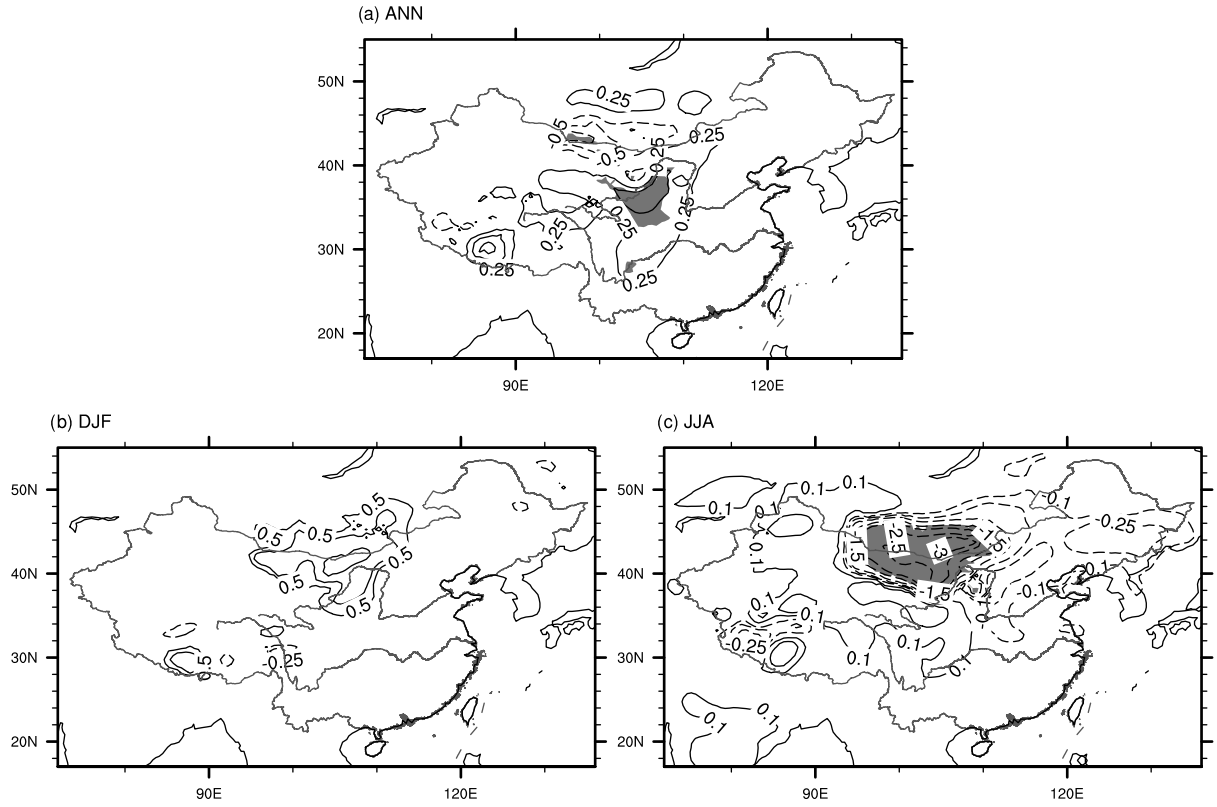

Figure 4. The (a) annual, (b) DJF and (c) JJA mean temperature differences (GRS−DST) between DST and GRS. Contour lines indicate the temperature difference (unit: °C); the shaded area indicates a statistically significant area at the 95% confidence level.

in vegetation are illustrated. The annual mean precipitation increased by 10–20% in the NWHP (Figure 6(a)), which was mainly caused by the increase in JJA precipitation. DJF precipitation increased in the NWHP and southeastern neighbouring areas (Figure 6(b)), but the increase was small in magnitude. The surface was bare and frozen during the winter (e.g. no obvious change in the surface upward latent heat flux in Figure 5(g)), so the change in precipitation was inconspicuous. In the summer, precipitation changes were evident on both local and regional scales. Locally, precipitation increased by more than 50%, and the increase was statistically significant. Previous analysis has shown that evapotranspiration over the NWHP area increased, which increased precipitation in advantageous weather conditions.

From Figures 4 and 6, we found that both local and remote climate responses were more apparent and significant in the summer. Therefore, we chose the changes in atmospheric circulation in the summer for further analyses on local and remote changes in precipitation. Figure 7 shows that the JJA geopotential height decreased in the lower troposphere but increased in the upper troposphere in the NWHP. Two main factors may be responsible for the temperature increase associated with the increase in geopotential height at higher levels: (1) evapotranspiration increases over the NWHP, so the moisture level reinforces the greenhouse gas warming effect, increasing the temperature in the middle troposphere; and (2) the surface temperature evidently decreases over the NWHP; hence, to maintain thermal balance, atmospheric warming exists in the middle troposphere. This increase in temperature in the middle troposphere was also found in the vertical profile of the JJA temperature difference in Figure 9.

In accordance with the decrease in geopotential height in the lower troposphere, there was a cyclonic circulation anomaly over NWHP. The vertical upward motion was intensified, so the geopotential height increased at middle and higher levels (Figure 7(h)). There was also an anticyclonic circulation anomaly over this region (Figure 8(h)).

Water-vapour transportation is an important source of moisture and precipitation. The JJA vapour transportation anomaly is shown in Figure 10. The water-vapour transported to the NWHP increased, which provided more warm moisture to the NWHP independent of the effect of the local increase in evapotranspiration. All of these factors were favourable for the increase in precipitation over the NWHP in the summer.

The mechanism for the local JJA precipitation change over the NWHP can be explained in the following manner. When the vegetation is changed from 'bare or sparsely vegetated' category to 'grassland,' albedo decreases, and downward and upward shortwave radiation at the surface decrease, but evapotranspiration and latent heat flux increases substantially because of the improved vegetation and soil conditions. The air moisture increases the water-vapour-induced greenhouse gas warming effect in the lower troposphere and warms the air, which leads to an increase in geopotential height at higher levels. The geopotential height at higher levels

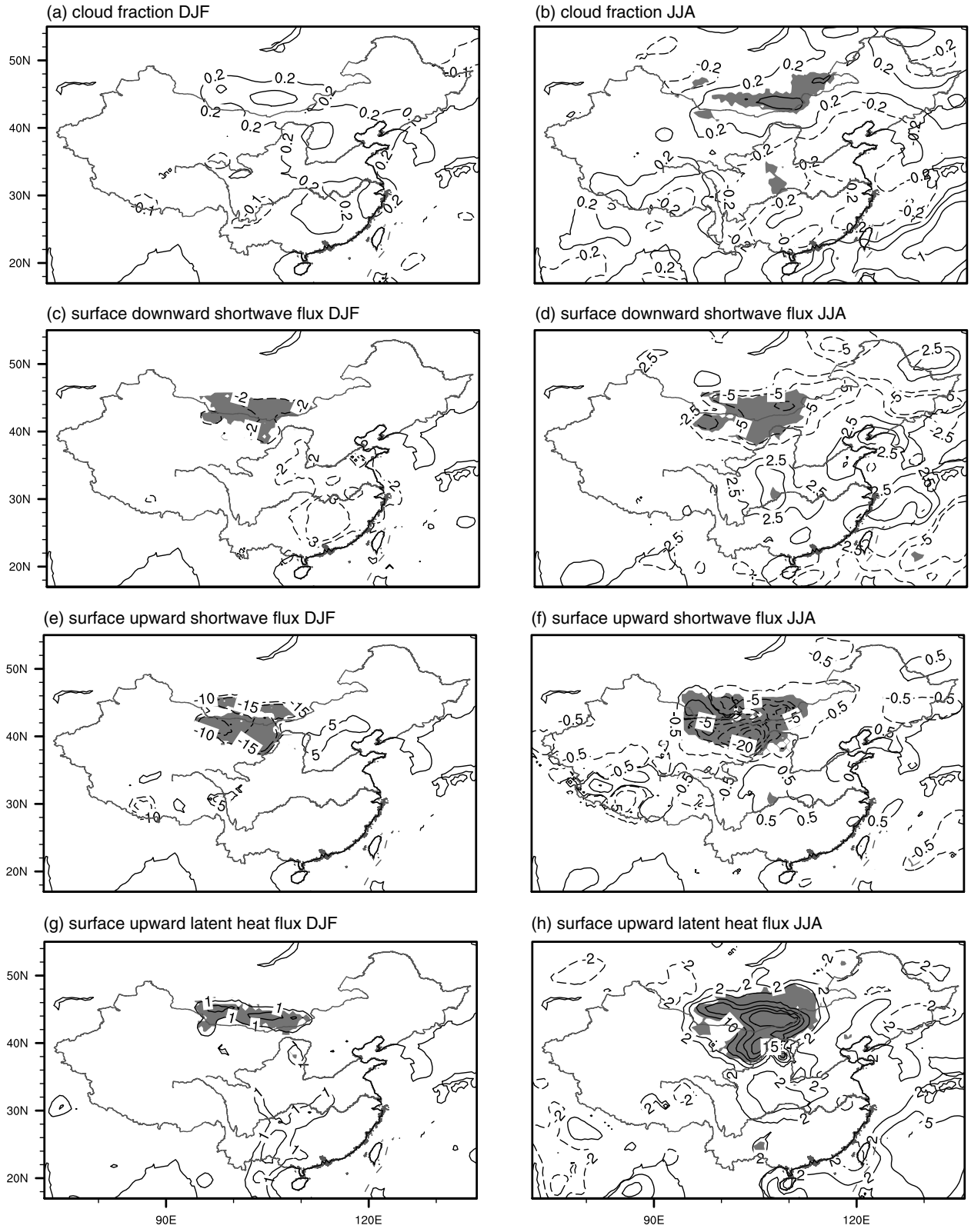

Figure 5. The DJF (left) and JJA (right) average GRS–DST difference for (a), (b) cloud fraction; (c), (d) surface downward shortwave flux; (e), (f) surface upward shortwave flux and (g), (h) surface upward latent heat flux.

increases, and there is a cyclonic circulation anomaly in the lower troposphere and an anticyclonic circulation anomaly at higher levels. These changes lead to higher atmospheric instability and intensified convection in the NWHP. At the same time, water-vapour transportation to this area also increases, resulting in an increase in precipitation in the summer.

The most remarkable feature of the JJA precipitation change is the large-scale response to changes in vegetation. We found that precipitation increases over

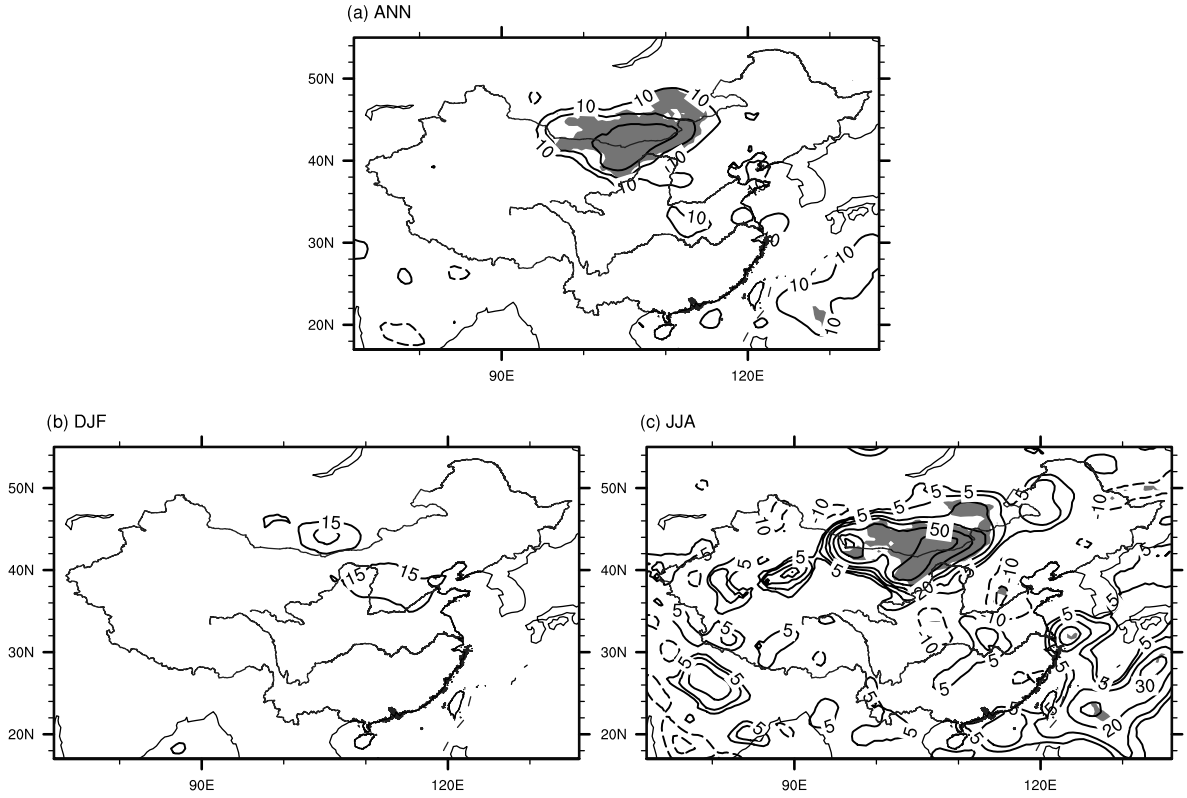

Figure 6. Same information as in Figure 4, except for (a) annual, (b) DJF and (c) JJA mean precipitation changes (%).

Central and South China and decreases over Central North China (Figure 6(c)). The geopotential height decreases in the lower troposphere and increases at higher levels over Central North China (Figure 7); accordingly, there is a cyclonic circulation anomaly at lower levels and an anticyclonic circulation anomaly at higher levels over this region (Figure 8). For Central and South China, a cyclonic circulation anomaly is present. With respect to water-vapour transportation, the transportation anomaly shows divergence (convergence) over Central North China (Central and South China), which is a disadvantageous (advantageous) factor for precipitation (Figure 10).

The background mechanism of the remote response is that the anticyclonic circulation anomaly in the middle and upper troposphere over North China causes a weakening of the East Asian Trough, the western Pacific subtropical high and the East Asian summer monsoon winds and eventually leads to an increase in precipitation over Central and South China and a decrease in precipitation over Central North China.

The present analysis shows the mechanism for local and regional changes in JJA precipitation. However, few studies have been focused on this type of regional-scale 'teleconnection.' Therefore, it is unclear whether this regional-scale teleconnection is the intrinsic mode of real atmospheric circulation.

We conducted the Empirical Orthogonal Functions (EOF) analysis of observational JJA geopotential height at the 500 hPa level for 1989–2009 using the NCEP reanalysis data set. Figure 11 shows the first principal component. We found that the value is negative over North China and positive over Central and South China, which means that if the geopotential height increases over North China, the geopotential height will decrease over Central and South China. Correspondingly, an anticyclonic circulation anomaly appears over North China, and a cyclonic circulation anomaly appears over Central and South China. This phenomenon coincides with our simulation and confirms the mechanism for the JJA precipitation change. The physical nature of this phenomenon can be explained by meridional Rossby wave patterns, as indicated by Nitta (1987) and Huang and Li (1989).

We can now summarize the previous analysis and suggest a possible mechanism to explain the local and remote climate responses to changes in vegetation in the summer over the NWHP shown in Figure 12. Locally, when the vegetation changes from 'bare or sparsely vegetated' category to 'grassland' over the NWHP, the albedo decreases, but evapotranspiration increases substantially, this leads to a decrease in the surface air temperature. The reinforced air moisture over the NWHP warms the air, which makes the geopotential height decrease at the lower level and increase at the higher level, and there is an anticyclonic circulation anomaly at higher levels. The atmospheric instability and convection in the NWHP increase, and water-vapour transportation to this area increases, causing an increase in precipitation in the summer. Remotely, the anticyclonic circulation anomaly at high tropospheric levels over North China causes a weakening of the East Asian Trough, weakening the western

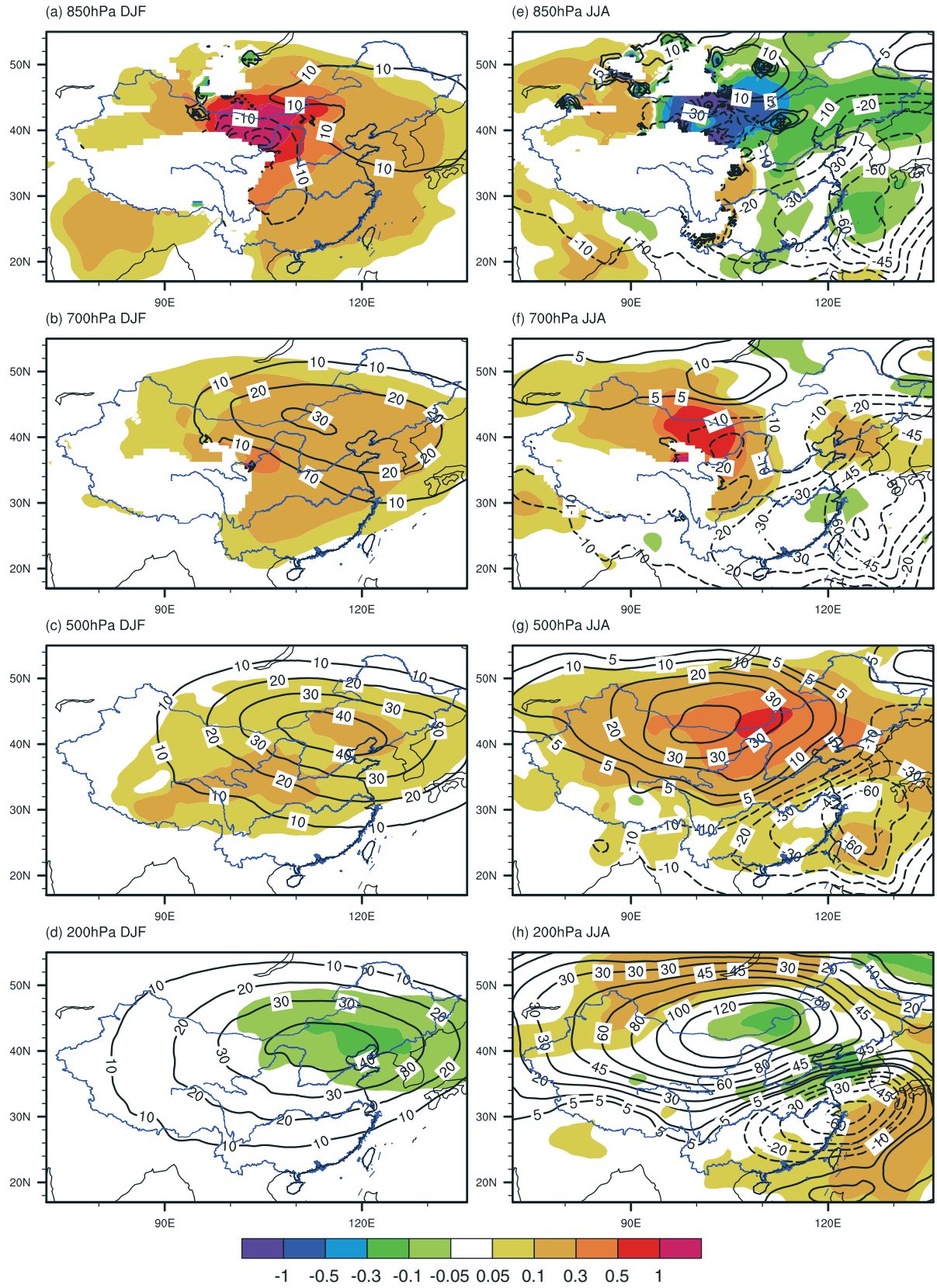

Figure 7. DJF (left) and JJA (right) mean geopotential heights (contour, GRS−DST, unit: gpm) and temperature (shaded, unit: °C) change at the levels of (a), (b) 850 hPa; (c), (d), 700 hPa; (e), (f) 500 hPa and (g), (h) 200 hPa.

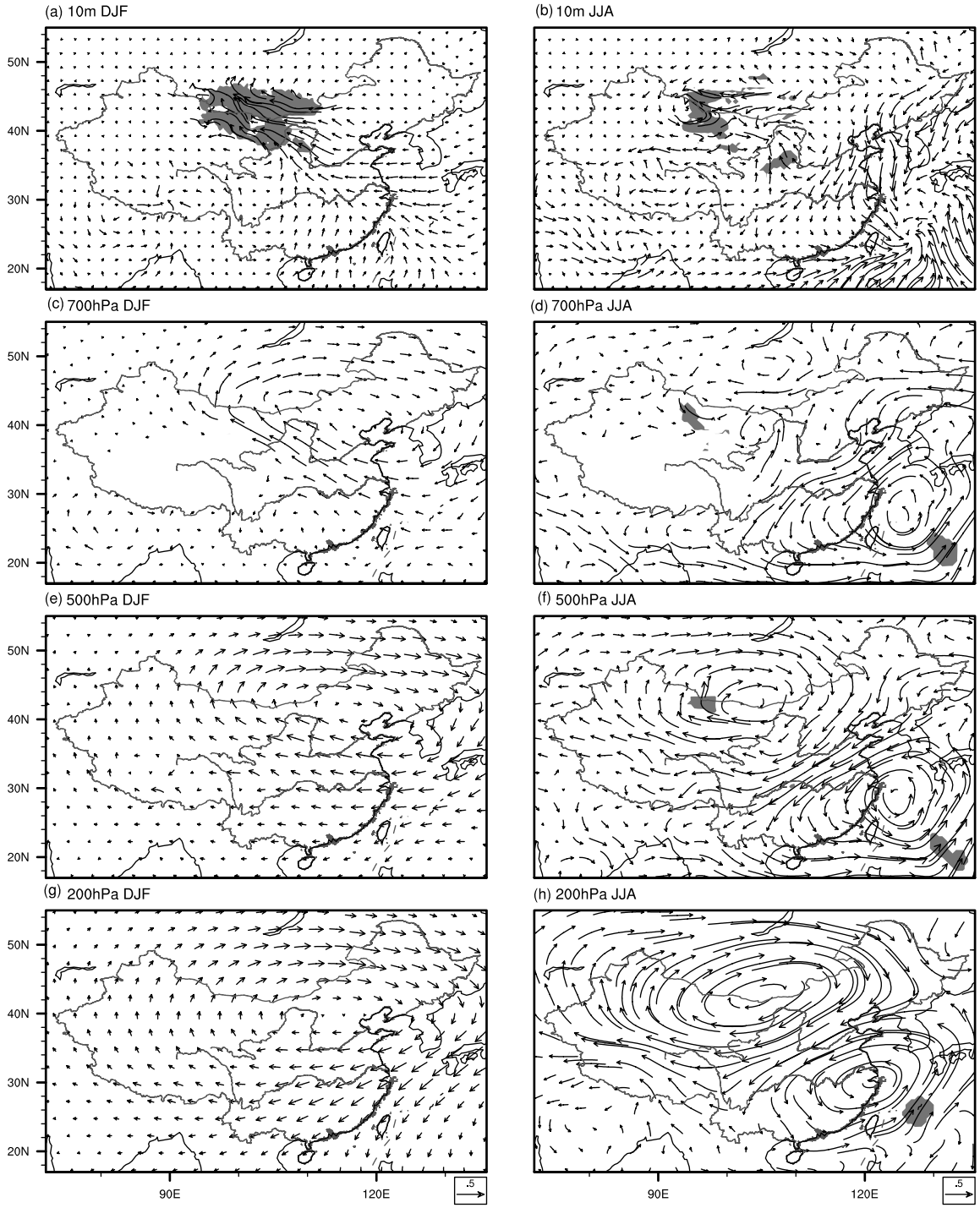

Figure 8. Same information as in Figure 7, but for wind at (a), (b) 10 m; (c), (d), 700 hPa; (e), (f) 500 hPa and (g), (h) 200 hPa.

Pacific subtropical high and East Asian summer monsoon. Hence, precipitation increases over Central and South China and decreases over Central North China. This remote climate response partially follows the features of real atmospheric circulation anomaly patterns, as indicated by the first EOF mode.

4. Conclusion and discussion

In this study, the climatic response to prescribed vegetation changes was investigated using the WRF model. The vegetation of the NWHP area was changed from 'bare or sparsely vegetated' to 'grassland.' When the vegetation changes, on a local scale, DJF temperature increases while JJA temperature decreases. Precipitation increases slightly in the winter and significantly in the summer. At the same time, a remote climatic response in the summer is also evident, as precipitation increases over Central and South China but decreases over Central North China. The geopotential height decreases in the lower troposphere, increases at higher levels over North China, and decreases across all levels over Central and South China.

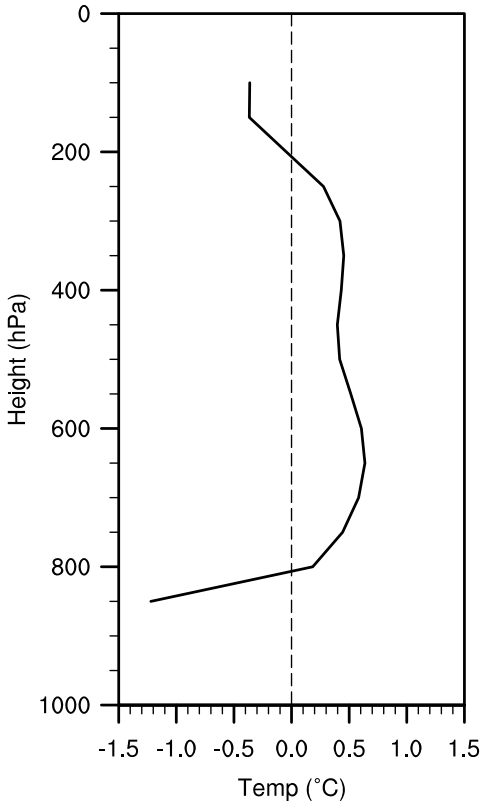

Figure 9. Vertical profile of the JJA temperature difference (GRS–DST, unit: °C).

Accordingly, there is a cyclonic circulation anomaly at lower levels, an anticyclonic circulation anomaly at higher levels over Central North China and an anomalous cyclonic circulation over Central and South China.

Our study describes the remote responses of local changes in vegetation. Naturally, these local changes in vegetation should occur on a sufficient spatial scale. Otherwise, they could not induce a remote response. Our conclusion could be useful in relevant ecological and environmental reconstruction efforts, particularly in

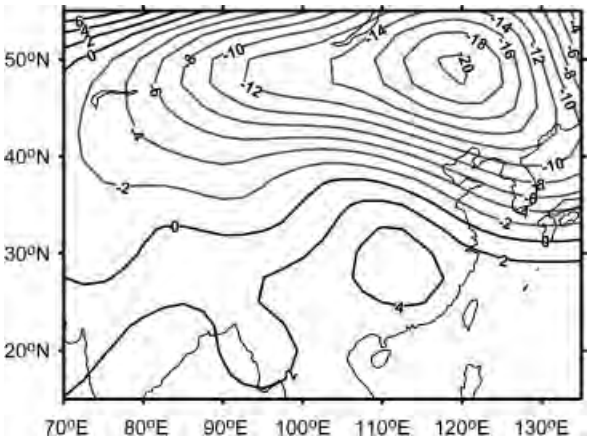

Figure 11. EOF1 of JJA geopotential height anomalies at the 500 hPa level for 1989–2009.

semi-arid or arid regions, as these regions are very environmentally sensitive.

This work is a preliminary study. Additional studies should be conducted to increase the robustness of these results. For example, in our study, only the influence of vegetation on climate was considered. The feedback of climate on vegetation is also important, and the interactive feedback mechanisms between climate and vegetation require further investigation.

Acknowledgements

This work was supported by the Major State Basic Research Development Program of China (973 Program) under Grant 2009CB421406, the National Natural Science Foundation of China under Grant 40875048 and 40821092, and Special Fund for Public Welfare Industry (meteorology) under Grant GYHY200906018. The use of observed high resolution temperature data (cn05) from National Climate Center of China and rain data from Tropical Rainfall Measuring Mission (TRMM) are acknowledged with thanks.

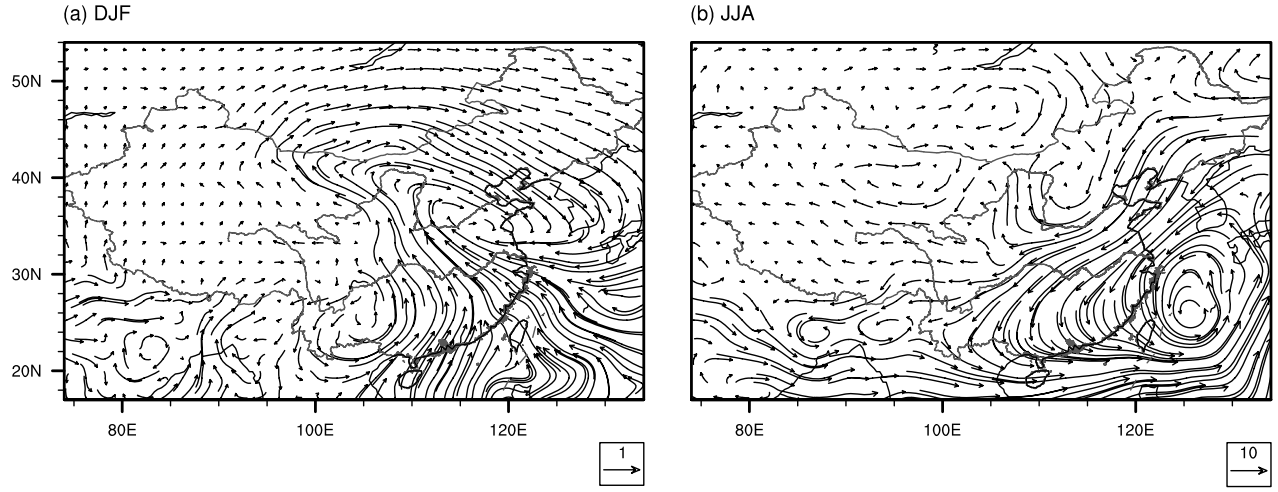

Figure 10. (a) DJF and (b) JJA averaged vapour transport differences (GRS–DST, unit: kg m^{-1} s^{-1}).

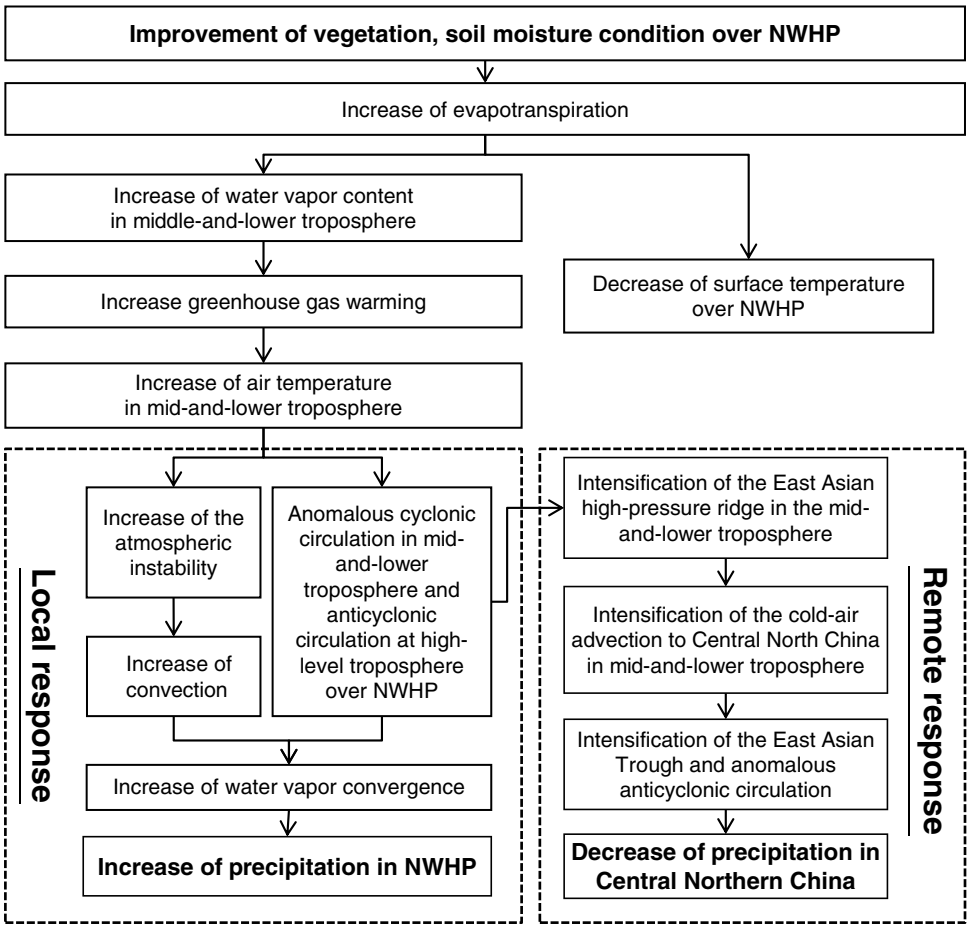

Figure 12. Conceptual map of the local and remote JJA climate responses to changes in vegetation in NWHP.

References

Anthes R, Kuo Y, Hsie E, Lownam S, Bettge T. 1989. Estimation of skill and uncertainty in regional numerical-models. *Quarterly Journal of the Royal Meteorological Society* **115**: 763–806.

Barstad I, Sorteberg A, Flatøy F, Déqué M. 2009. Precipitation, temperature and wind in Norway: dynamical downscaling of ERA40. *Climate Dynamics* **33**: 769–776.

Bollasina M, Nigam S. 2011. Modeling of regional hydroclimate change over the Indian subcontinent: impact of the expanding Thar desert. *Journal of Climate* **24**: 3089–3106.

Bonan GB. 1997. Effects of land use on the climate of the United States. *Climatic Change* **37**: 449–486.

Charney J. 1975. Dynamics of deserts and drought in the Sahel. *Quarterly Journal of the Royal Meteorological Society* **101**: 193–202.

Chen F, Dudhia J. 2001. Coupling an advanced land surface-hydrology model with the Penn State-NCAR MM5 modeling system. Part I: model implementation and sensitivity. *Monthly Weather Review* **129**: 569–585.

Collins W, Rasch P, Boville B, Hack J, McCaa J, Williamson D, Kiehl J, Briegleb B, Bitz C, Lin S. 2004. Description of the NCAR Community Atmosphere Model (CAM 3.0). *NCAR Tech. Note NCAR/TN-464+ STR*.

Dickinson RE, Henderson-Sellers A. 1988. Modelling tropical deforestation: a study of GCM land-surface parametrizations. *Quarterly Journal of the Royal Meteorological Society* **114**: 439–462.

Ding YH, Li QP, Dong WJ. 2005. A numerical simulation study for the study of the impacts of vegetation changes on regional climate in China. *Acta Meteorologica Sinica* **63**: 613–621.

Fan GZ, Lv SH, Luo SW. 1998. The influence of the NW China afforestation on regional climate in East and South Asia. *Plateau Meteorology* **17**: 300–308.

Fu C. 2003. Potential impacts of human-induced land cover change on East Asia monsoon. *Global and Planetary Change* **37**: 219–229.

Fu C, Yuan H. 2001. An virtual numerical experiment to understand the impacts of recovering natural vegetation on the summer climate and environmental conditions in East Asia. *Chinese Science Bulletin* **46**: 1199–1203.

Gao XJ, Luo Y, Lin WT, Zhao ZC, Filippo G. 2003. Simulation of effects of land use change on climate in China by a regional climate model. *Advances in Atmospheric Sciences* **20**: 583–592.

Gao XJ, Zhang DF, Chen ZX. 2007. Numerical simulation of impacts of landuse over China. *Chinese Science Bulletin* **37**: 397–404.

Gemmill W, Katz B, Li X. 2007. Daily real-time global sea surface temperature-high resolution analysis at NOAA/NCEP. *MMAB Official Note* **260**: 39 pp.

Hong SY, Dudhia J, Chen SH. 2004. A revised approach to ice microphysical processes for the bulk parameterization of clouds and precipitation. *Monthly Weather Review* **132**: 103–120.

Hong SY, Lim JOJ. 2006. The WRF single-moment 6-class microphysics scheme (WSM6). *Journal of the Korean Meteorological Society* **42**: 129–151.

Hong SY, Noh Y, Dudhia J. 2006. A new vertical diffusion package with an explicit treatment of entrainment processes. *Monthly Weather Review* **134**: 2318–2341.

Huang RH, Li L. 1989. Numerical simulation of the relationship between the anomaly of subtropical high over East Asia and the convective activities in the western tropical Pacific. *Advances in Atmospheric Sciences* **6**: 202–214.

Huffman GJ, Adler RF, Morrissey MM, Bolvin DT, Curtis S, Joyce R, McGavock B, Susskind J. 2001. Global precipitation at one-degree daily resolution from multisatellite observations. *Journal of Hydrometeorology* **2**: 36–50.

IPCC. 2007. *Regional Climate Projections. Climate Change 2007: The Physical Science Basis. Contribution of Working Group I to the Fourth Assessment Report of the Intergovernmental Panel on Climate Change*. Cambridge University Press: Cambridge, United Kingdom and New York, NY, USA; 884.

Jiang DB, Wang SG, Liang XM, Dong GR, Shang KZ, Yang DB. 2001. Influence of desertification on climate in desert region of China. *Journal of Desert Research* **21**: 428–432.

Jiang DB, Wang SG, Liang XM, Dong GR, Shang KZ, Yang DB. 2003. Influence of afforestation on climate in desert region of China. *Journal of Desert Research* **23**: 63–66.

Kain J. 2004. The Kain–Fritsch convective parameterization: an update. *Journal of Applied Meteorology* **43**: 170–181.

Kain J, Fritsch J. 1993. Convective parameterization for mesoscale models: The Kain–Fritsch scheme. The representation of cumulus convection in numerical models. *Meteorological Monograph* **46**: 165–170.

Lean J, Warrilow DA. 1989. Simulation of the regional climatic impact of Amazon deforestation. *Nature* **342**: 411–413.

Li JX, Shi XQ. 2009. The analysis of trends and characteristics of climate evolution from 1961 to 2000 in Zhalot Banner. *Yinshan Academic Journal* **23**: 43–49.

Lo JC, Yang ZL, Pielke RA, Sr. 2008. Assessment of three dynamical climate downscaling methods using the Weather Research and Forecasting (WRF) model. *Geophysical Research Letters* **113**: D09112.

Mukhopadhyay P, Taraphdar S, Goswami B, Krishnakumar K. 2010. Indian summer monsoon precipitation climatology in a high-resolution regional climate model: impacts of convective parameterization on systematic biases. *Weather and Forecasting* **25**: 369–387.

Nitta T. 1987. Convective activities in the tropical western Pacific and their impact on the Northern Hemisphere summer circulation. *Journal of the Meteorological Society of Japan* **65**: 373–390.

Nobre C, Sellers P, Shukla J. 1991. Amazonian deforestation and regional climate change. *Journal of Climate* **4**: 957–988.

Pielke RA, Adegoke J, Beltran-Przekurat A, Hiemstra CA, Lin J, Nair US, Niyogi DS, Nobis TE. 2007. An overview of regional land use and land cover impacts on rainfall. *Tellus* **59B**: 587–601.

Pielke RA, Marland SG, Betts RA, Chase TN, Eastman JL, Niles JO, Niyogi DS, Running SW. 2002. The influence of land-use change and landscape dynamics on the climate system: relevance to climate-change policy beyond the radiative effect of greehouse grases. *Philosophical Transactions of the Royal Society of London* **B360**: 1705–1719.

Qian Y, Ghan SJ, Leung LR. 2010. Downscaling hydroclimatic changes over the Western US based on CAM subgrid scheme and WRF regional climate simulations. *International Journal of Climatology* **30**: 675–693.

Shukla J, Nobre C, Sellers P. 1990. Amazon deforestation and climate change. *Science* **247**: 1322.

Skamarock W, Klemp J, Dudhia J, Gill D, Barker D, Duda M, Huang X, Wang W, Powers J. 2008. *A description of the advanced research WRF version 3*.

Sud YC, Molod A. 1988. A GCM simulation study of the influence of Saharan evapotranspiration and surface-albedo anomalies on July circulation and rainfall. *Monthly Weather Review* **116**: 2388–2400.

Wang HJ. 1999. Role of vegetation and soil in the Holocene megathermal climate over China. *Journal of Geophysical Research* **104**: 9361–9367.

Xu Y, Gao X, Shen Y, Xu C, Shi Y, Giorgi aF. 2009. A daily temperature dataset over China and its application in validating a RCM simulation. *Advance in Atmospheric Sciences* **26**: 763–772.

Xue Y. 1996. The impact of desertification in the Mongolian and the inner Mongolian grassland on the regional climate. *Journal of Climate* **9**: 2173–2189.

Xue Y, Shukla J. 1993. The influence of land surface properties on Sahel climate. Part 1: desertification. *Journal of Climate* **6**: 2232–2245.

Xue Y, Shukla J. 1996. The influence of land surface properties on Sahel climate. Part II: afforestation. *Journal of Climate* **9**: 3260–3275.

Zeng XD. 2010. Evaluating the dependence of vegetation on climate in an improved dynamic global vegetation model. *Advances in Atmospheric Sciences* **27**: 977–991.

Zhang H, Henderson-Sellers A, McGuffie K. 1996a. Impacts of tropical deforestation. Part I: process analysis of local climatic change. *Journal of Climate* **9**: 1497–1517.

Zhang H, McGuffie K, Henderson-Sellers A. 1996b. Impacts of tropical deforestation. Part II: the role of large-scale dynamics. *Journal of Climate* **9**: 2498–2521.

